ACADEMIC PRESS

Available online at www.sciencedirect.com

SCIENCE DIRECT®

Journal of Magnetic Resonance 161 (2003) 70–76

JMR Journal of Magnetic Resonance

www.elsevier.com/locate/jmr

Flow encoded NMR spectroscopy for quantification of metabolite flow in intact plants

Michael Szimtenings, Silvia Olt,* and Axel Haase

Physikalisches Institut, Lehrstuhl für Experimentelle Physik V (Biophysik), Universität Würzburg, Am Hubland, Würzburg 97074, Germany

Received 25 July 2002; revised 19 November 2002

Abstract

An NMR flow quantification technique applicable to metabolite flow in plants is presented. It combines flow sensitive magnetization preparation with slice selective spectroscopy. Flow encoded NMR spectroscopy is described to quantify, for the first time, flow velocities of metabolites in plants non-invasively. Flow sensitivity is introduced by magnetization preparation based on a stimulated echo experiment, prior to slice selective spectroscopy. For flow quantification eight different flow-weighted spectra are collected. With this flow preparation very slow flow velocities down to 0.1 mm/s can be detected and small amounts of flowing metabolites can be observed despite the large background signal of stationary and flowing water. Important sequence optimization steps include appropriate choice of experimental parameters used for flow encoding as well as complete balancing of eddy currents from the flow encoding gradients. The method was validated in phantom experiments and applied in vivo. Examples of quantitative flow measurements of water and metabolites in phantoms and plants are provided to demonstrate the reliability and the performance of flow encoded spectroscopy.

Keywords: NMR flow quantification; Spectroscopy; Plants; Microimaging

1. Introduction

NMR techniques are useful tools for studying transport processes in plants. Using ^{13}C-labeled tracers in combination with indirect detection methods the carbohydrate uptake in living plants was observed [1]. The ability of NMR flow imaging to measure water flow in plants has been reported by several authors [2–8]. However, so far it has not been possible to measure the flow velocity of metabolites directly. Here, a spectroscopic approach for NMR flow quantification is chosen. For this, we combine a flow encoding preparation experiment with slice selective spectroscopy. The proposed method provides another feature: as phloem and xylem signal are discerned spectroscopically, phloem flow is accessible even if xylem and phloem are physically located too close together to be separated in NMR-images. In contrast to this, NMR flow imaging can only measure phloem flow in the rather rare plant species where the phloem is distant from the xylem region [9], whenever a full propagator approach [7] is not used.

Flow quantification of metabolites in plants is challenging: typical flow velocities are in the range of 500 μm/s and in general a very low concentration of flowing metabolites has to be detected in the presence of a large water signal. To meet these requirements, the timing of the flow encoding sequence has to be tailored with respect to the diffusion and NMR relaxation time constants of the metabolite of interest. Special care has to be taken to compensate eddy currents from the flow encoding gradients, otherwise these eddy currents result in a false flow signal in the spectroscopic experiment.

Regarding the quantification of slow flow velocities, the accuracy of the proposed technique is demonstrated in a phantom study using a tube with flowing ethanol. The capacity to detect also low concentrations of flowing metabolites in the presence of flowing and stationary water is proven in a second phantom study. The phantom models a plant stem in terms of dimensions, concentrations and flow velocities. As a first in vivo

* Corresponding author. Fax: +49-931-706-297.
E-mail address: saolt@physik.uni-wuerzburg.de (S. Olt).

1090-7807/03/$ - see front matter © 2003 Elsevier Science (USA). All rights reserved.
doi:10.1016/S1090-7807(02)00183-0

application, 50-day-old *Ricinus communis* plants were investigated. Consciously, a plant species was chosen, whose xylem and phloem are located in different regions. In this plant, NMR flow imaging has already been applied to determine the water flow velocity in the phloem [9] and the results from this study could be compared to those acquired previously. Additionally, 2D chemical shift imaging (CSI) was performed providing spatial information about the metabolites under investigation.

2. Theoretical background

According to the concept of magnetization preparation in NMR microscopy [10], flow encoded spectroscopy comprises two completely decoupled parts: flow encoding as the preparation part and slice selective spectroscopy as the read-out part.

2.1. Flow sensitive magnetization preparation

Since low velocities have to be encoded, but in plants the longitudinal relaxation time constant T_1 is considerably longer than the transverse relaxation time constant T_2, a stimulated echo experiment was used for flow encoding (Fig. 1). First proposed by Bourgeois [11] as a flow sensitive preparation strategy, this technique offers the advantage that the magnetization is stored longitudinally during the gradient pulse separation time T. As shown in Fig. 1 the stimulated echo is produced by three $90°_x$ pulses. At the time of the stimulated echo the magnetization vector of the stationary spins M_{stat} points along the into the y-direction, whereas the magnetization of moving spins M_{flow} has accumulated a phase depending on the flow velocity v, the strength of the velocity encoding gradients G and the time delays τ and T [14]

$$\varphi = -\gamma G\tau(T+\tau)v. \tag{1}$$

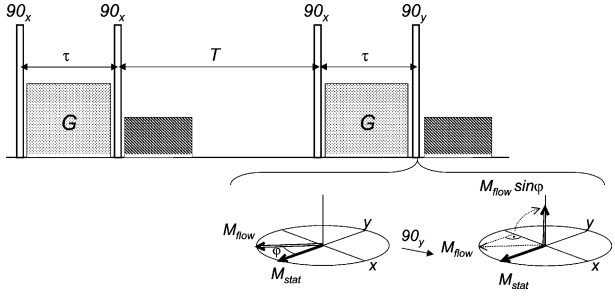

Fig. 1. Flow encoding for magnetization preparation on the basis of a stimulated echo experiment. The sequence comprises four r.f. pulses and two flow encoding gradients. After the second and the fourth r.f. pulse dephasing gradients are applied to destroy the transverse magnetization. Ideally, the preparation results in flowing magnetization only being stored in the longitudinal direction.

At this time, a fourth RF pulse is applied ($90°_y$), which leaves the stationary magnetization unaffected and flips the x-component of the flowing magnetization back along the longitudinal direction. It shows an oscillating behavior

$$M_{\text{prep}} \propto M_{\text{flow}} \sin(\gamma G\tau(T+\tau)v) \tag{2}$$

and is now read out by the following slice-selective spectroscopic experiment. The remaining transverse magnetization is removed by a spoiler gradient.

A simple control experiment can be performed by switching the r.f. phase of the fourth pulse: A $90°_x$ pulse, instead of a $90°_y$ pulse, acts on the stationary magnetization (and on the y-component of the flowing magnetization). Under these circumstances primarily stationary signal is detected. Whenever an expected spectral line is absent in the flow encoded spectra, this control experiment can be used to check whether the corresponding metabolite is in fact stationary, or whether no signal is detected due to low low sensitivity.

So far, only plug flow has been considered. In the plant, several vessels—each with a laminar flow profile—contribute to the signal. Besides this, we assume that the average velocity v_{avg} in all vessels contributing to the signal is the same. In this case, Eq. (3) has to be replaced by [11]

$$M_{\text{prep}} \propto M_{\text{flow}} \frac{\sin^2(\gamma G\tau(T+\tau)v_{\text{avg}})}{\gamma G\tau(T+\tau)v_{\text{avg}}}. \tag{3}$$

2.2. Off-resonance effects

In this bipolar flow-encoded experiment flowing spins acquire a flow related, but chemical shift independent phase. Due to the time symmetry of the pulse sequence fully flow encoded spectral information is preserved over the whole spectral range.

2.3. Signal attenuation due to relaxation and diffusion

Signal attenuation caused by relaxation and diffusion has to be taken into account. During the time intervals τ, the magnetization is transverse and T_2-decay occurs, during T the magnetization is stored in the longitudinal direction and relaxes with T_1. Knowing the diffusion constant D, the signal loss due to diffusion can be described by the Stejskal–Tanner equation [12]. Therefore, the full signal dependence is given by

$$M_{\text{prep}} \propto M_{\text{flow}} \times \frac{\sin^2(\gamma G\tau(T+\tau)v_{\text{avg}})}{\gamma G\tau(T+\tau)v_{\text{avg}}} \underbrace{e^{-\gamma^2G^2\tau^2D(T+(2/3)\tau)}}_{\text{Diffusion}} \underbrace{e^{-(2\tau/T_2)-(T/T_1)}}_{\text{Relaxation}}. \tag{4}$$

2.4. Flow quantification and model function

For flow quantification a series of N flow encoded spectra are acquired while the strength of the flow encoding gradient is increased up to a value $G_{\max}$. Since τ and T are identical for all flow encoding steps, the influence of relaxation remains the same and can be disregarded in the function describing the signal behavior. In contrast to this, the signal loss caused by diffusion has to be incorporated into the model function

$$S(q) \propto \frac{\sin^2(qv_{\text{avg}})}{qv_{\text{avg}}} e^{-q^2\tilde{D}} \tag{5}$$

with

$$q = \gamma G\tau(T+\tau),$$
$$\tilde{D} = \frac{T+(2/3)\tau}{(T+\tau)^2} D.$$

Provided that the diffusion constant of the metabolite of interest is known, a fit of the series of spectra using this function results in the average flow velocity.

2.5. Detectable velocity range and sensitivity

Since the model function $\sin^2(x)/x$ has to be at least sampled up to the first maximum, a given set of experimental parameters τ, T, and $G_{\max}$ automatically defines the lower limit of the velocity to be recorded:

$$v_{\text{nom}} = \frac{0.37\pi}{\gamma G_{\max}\tau(T+\tau)}. \tag{6}$$

With N flow encoding steps the maximum, non-aliased velocity is determined by the Nyquist theorem [13]

$$v_{\max} = Nv_{\text{nom}}. \tag{7}$$

In practice, signal attenuation due to relaxation and diffusion has to be taken into account and τ and T cannot be chosen to be arbitrarily long. An inherent limit is given by the fact that the distance propagated during the longest possible duration of observation has to exceed the motion due to diffusion. Here, the longest possible observation time $(T+\tau)$ is of the order of T_1. Thus, the slowest observable velocity is given by [14]

$$v_{\min} \approx \sqrt{\frac{D}{T_1}}. \tag{8}$$

To minimize signal loss, experimental parameters τ and T have to be chosen appropriately. In principle, the optimum values for τ and T can be derived analytically from Eq. (3) within the constraints of Eq. (6). In the same way, the expected signal loss due to diffusion and relaxation can be predicted. Of course, knowledge of the diffusion constant D and the relaxation times T_1 and T_2 in vivo are required for this purpose.

3. Materials and methods

3.1. Sequence optimization

Fig. 2 schematically shows the entire sequence used in this study.

3.1.1. Destruction of remaining longitudinal magnetization

The repetition time of the experiment is significantly shorter than typical T_1 values of water in plants. To ensure a well defined initial state of the magnetization for each scan, the remaining longitudinal magnetization is destroyed at the end of each repetition. To this end a combination of a $90°_x$ and a $180°_y$ pulse and a dephasing gradient is applied three times (see also Fig. 2).

3.1.2. Balance of eddy currents

The spectroscopic experiment turned out to be highly sensitive to eddy currents from the previously applied flow encoding gradients. This problem could be resolved by switching an additional gradient pulse of the same strength but opposite polarity prior to each of the flow encoding gradient pulses, as shown in Fig. 2. Since these gradients are applied when the magnetization from flowing spins is longitudinal, they have no encoding effect. In this manner, all eddy currents of the flow encoding part of the sequence are balanced [17].

3.1.3. Gradient and r.f. phase cycling

A eight element gradient and r.f. phase cycle ensures the complete cancellation of the stationary signal. For gradient cycling [15], the polarity of the flow encoding gradient is inverted in conjunction with an inversion of the acquisition phase. This is combined with CYCLOPS [16] phase cycling of the spectroscopy part of the sequence (see also Table 1).

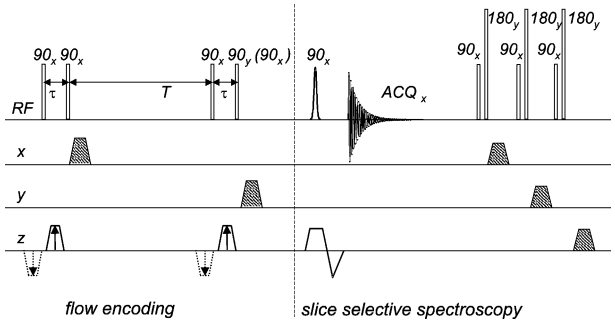

Fig. 2. The full sequence for flow encoded spectroscopy comprises two parts: flow encoding and slice selective spectroscopy. The gradient pulses shown as dashes were incorporated to compensate eddy currents from the flow encoding gradient pulses: they do not have encoding properties themselves. Depending on the r.f. phase of the fourth pulse of the flow encoding part, a flow encoded experiment (90_y) or a control experiment (90_x) is performed. At the end of each repetition, the remaining longitudinal magnetization is destroyed by three combinations of a $90°_x$ and a $180°_y$ pulse and a dephasing gradient.

Table 1
The eight element phase cycle used for complete cancellation of the stationary signal in flow encoded spectroscopy

Gradient polarity	r.f. phase of excitation pulse	Acquisition phase
+	$+x$	$+x(+x)$
−	$+x$	$-x(+x)$
+	$+y$	$+y(+y)$
−	$+y$	$-y(+y)$
+	$-x$	$-x(-x)$
−	$-x$	$+x(-x)$
+	$-x$	$-y(-y)$
−	$-x$	$+y(-y)$

To perform a control experiment, the acquisition phase as to be adapted as indicated in parenthesis.

3.2. Experimental

All experiments were performed on a 7 T Bruker BIOSPEC 70/20 horizontal bore magnet. The actively shielded gradient coils are capable of maximum gradient strengths of 196 mT/m with a minimum rise time of 240 μs. A homebuilt climate chamber [4] ensures optimum environmental conditions for the plants investigated and enables illumination and climate control. The r.f. coil acting as transmitter and receiver within this chamber can be interchanged. Helmholtz-type coils of different sizes (10–12 mm diameter) adapted to the diameter of the plant/phantom were used. The duration of the 90° hard pulse was 10 μs.

To quantify the flow velocity, eight flow encoding steps were performed uniformly increasing the gradient strength of the flow encoding gradients. Flow encoding parameters were adjusted so that the lower limit of the detectable velocity range was 109 μm/s. Due to limitations of the gradient hardware the maximum gradient strength applied was 172 mT/m. The timing of the flow encoding part was optimized assuming τ and T were chosen as 2.403 and 93 ms.

For slice selective spectroscopy, a 500 μs Gaussian-shaped pulse with a flip angle of 90° was chosen as the excitation pulse. The slice thickness was 5 mm. Five hundred and twelve complex data points were sampled with a 10 ppm sweep width placed symmetrically about the water resonance. The whole experiment was averaged 32 times using the eight step gradient and r.f. phase cycling described above. Data from each step of the cycle were saved to disk separately and coadded after post-processing correction. Using eight flow encoding steps, each with eight scans, the whole data set comprised 64 FIDs. Using a 1.2 s repetition time, the total measurement time was about 42 min.

3.3. Data processing

The acquired data were transferred to a PC and automatically processed with customized IDL routines. After baseline correction an exponential time-domain filter (filter width = 10 Hz) was applied. The filtered FIDs were zerofilled by a factor of 16 prior to Fourier transformation. According to the peak position of the water resonance in the corresponding magnitude spectra, the complex spectra were realigned to correct for any spectral shift induced by remaining eddy-currents. After multiplication of the spectra with a constant phase factor determined from the water peak, the spectra belonging to the same phase cycle were added up. The result is a set of eight flow-weighted spectra. Integration over the spectral range corresponding to the resonance of interest was performed. Finally, data were fitted using an appropriate function according to Eq. (5).

3.4. The phantoms

For the validation of flow quantification a tube with 1.05 mm inner diameter was used as a phantom. As the flowing fluid ethanol was pumped at four different velocities between 0.3 and 3 mm/s. In parallel, flow velocity was determined by volume calibration. In this case, apart from the eight element phase cycling, no additional averaging was necessary. For flow evaluation the spectral line at 1.11 ppm was selected. The diffusion constant for ethanol at 25 °C ($D = 1.1 \times 10^{-5}\,\mathrm{cm}^2/\mathrm{s}$) was taken from the literature [18].

A second phantom, modelling a plant stem, comprises three tubes. The outer 5 mm diameter tube is filled with stationary water. Two smaller tubes are put inside, a 0.87 mm diameter "xylem vessel" with water flowing at 580 μm/s and a 0.76 mm diameter "phloem vessel" with 100 mM sucrose flowing at 390 μm/s. The flow in the two tubes is in opposite directions. For comparison, spin-echo flow imaging [19] was performed to map the flow velocity of water and a CSI data set was collected providing the sucrose distribution.

3.5. The plant model

Ricinus communis plants, about 50 days old, were grown in quartz sand [20]. At this age, the size of the plant is about 30 cm, their originally discrete eight vascular bundles have already grown together and form a ring, but the xylem region is still spatially separated from the phloem region. The investigated slice of hypocotyl was chosen 8 cm above the sand surface. Fig. 6(b) shows a high resolution NMR spin-echo image of this slice. The cortex, phloem, xylem and pith parenchyma can be distinguished in great detail.

After flow encoded spectroscopy NMR flow imaging of the plant was performed. Subsequently, a

2D spin-echo CSI data set was acquired, which served as anatomical reference giving the spatial distribution of the metabolites belonging to the observed resonances.

4. Results

4.1. Phantom studies

The flow velocities of ethanol in the tube phantom calculated from slice selective spectroscopy (v_{NMR}) and those derived from volume calibration (v_{VC}) were in good agreement over the whole investigated velocity range. Fig. 3 compares the results of both techniques. A linear fit of the data gave the calibration curve:

$$v_{VC} = (1.09 \pm 0.04)\ v_{NMR} + (0.00 \pm 0.05)\,\mathrm{mm/s}. \qquad (9)$$

The errors indicated here and for all other parameters in the paper are standard deviations. In Fig. 4 the results of the experiments on the plant phantom are shown. The metabolite map calculated from a CSI data set in Fig. 4(d) monitors the sucrose in the "phloem" tube. The set of eight different flow weighted spectra is shown in Fig. 4(a). At 3.7 ppm a resonance of sucrose can be observed. The dependence of the signal intensity of this spectral line as a function of flow encoding is shown in Fig. 4(b). The flow velocity of sucrose derived from these data ($390 \pm 23\,\mu\mathrm{m/s}$) matches very well the flow

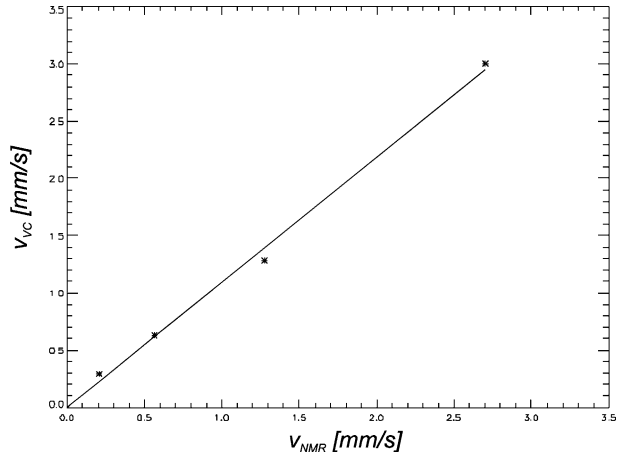

Fig. 3. Flow encoded spectroscopy versus volume calibration: a comparison of four different flow velocities of ethanol in a tube phantom measured with both methods.

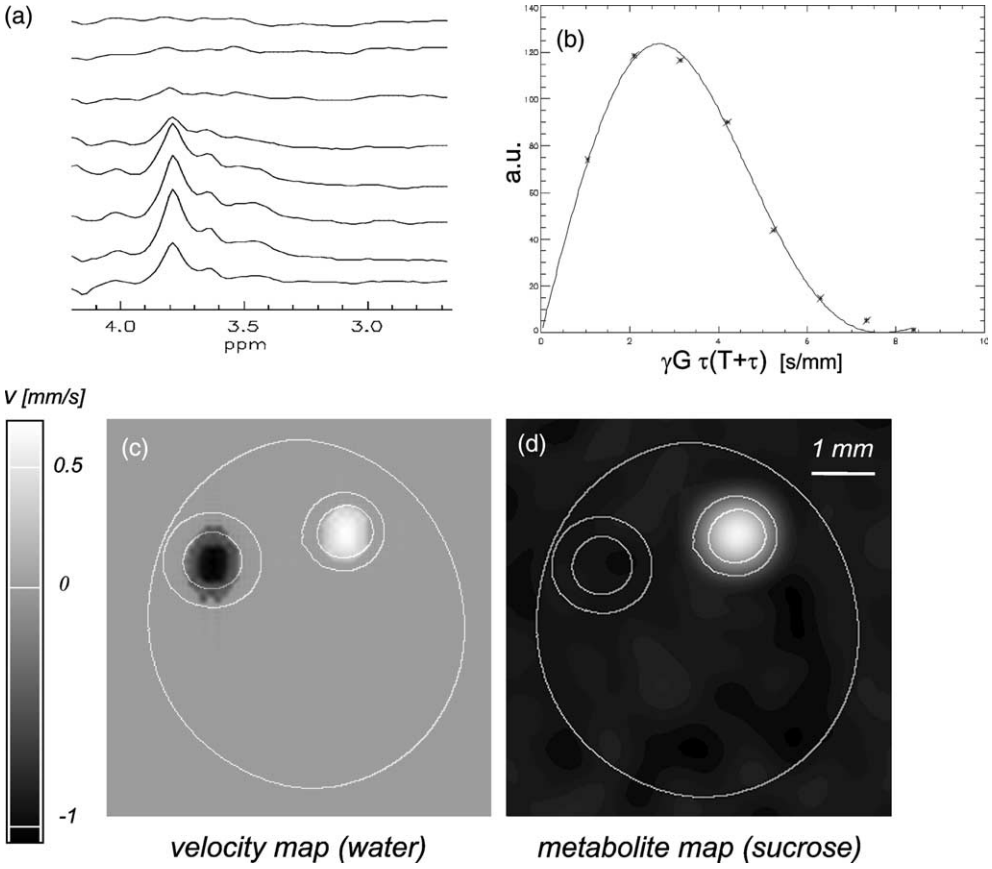

Fig. 4. Plant phantom. Flow encoded spectra (a). The spectral range around the resonances of sucrose at 3.7 ppm is shown. Signal course of the sucrose resonance at 3.7 ppm as a function of flow weighting (b) derived from (a). The solid line shows the fit of the model function, giving the flow velocity of sucrose. A velocity map of water obtained by spin-echo flow imaging (c) and a metabolite map derived from a CSI data set (d) monitor the distribution of flowing water and sucrose, respectively.

Table 2
Plant phantom: flow velocities in μm/s obtained by flow spin-echo imaging and flow encoded spectroscopy compared to those obtained by volume alibration

	Volume calibration	Flow imaging (water)	Flow encoded spectroscopy (sucrose)
"Xylem" tube	-580 ± 73	-540 ± 8	—
"Phloem" tube	390 ± 49	340 ± 5	390 ± 23

velocity of the fluid in the "phloem" tube obtained by volume calibration ($390 \pm 49\,\mu m/s$). By means of NMR flow imaging, the water flow velocity was also measured. In the velocity map in Fig. 4 the "xylem" tube with water and the "phloem" tube with 100 mM sucrose flowing in opposite directions can be clearly discerned. Table 2 compares the velocity values obtain with all three methods. Flow encoded spectroscopy and volume calibration are in very good agreement, whereas flow imaging slightly underestimates the flow velocity.

4.2. Plants

In the flow encoded spectra of *R. communis*, in addition to the water resonance, two spectral lines

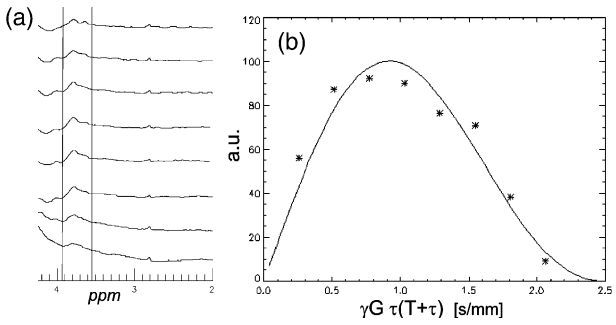

Fig. 5. Set of flow encoded spectra of the hypocotyl of a *R. communis* plant. In the spectral range of interest a resonance at 3.7 ppm arising from flowing carbohydrates can be identified. Signal intensities of the carbohydrate resonance in the different flow weighted spectra and the fit of these data are shown in (b).

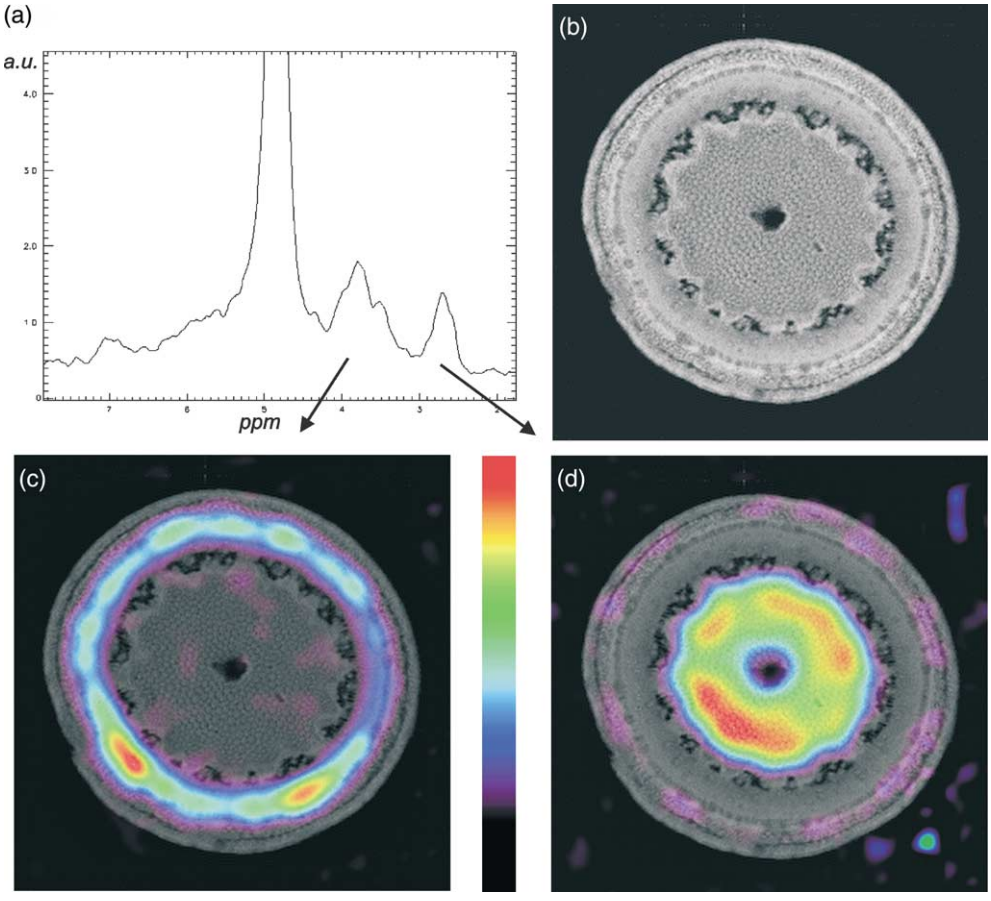

Fig. 6. Slice of the hypocotyl of *R. communis*. The spectrum (a) comprises, apart from the water signal, a carbohydrate resonance at 3.7 ppm and a resonance of an unidentified metabolite at 2.7 ppm. A high resolution spin-echo image (TE = 8 ms, TR = 1 s, FOV = $7 \times 7\,mm^2$, matrix = 256×256) of the slice is also shown (b). The metabolite maps of 3.7 ppm (c) and 2.7 ppm (d) superimposed on the corresponding spin-echo image were calculated from a CSI data set. While the carbohydrate is located in the phloem region, the unknown metabolite occurs in the parenchyma only.

were observed. The spectral range of interest is shown in Fig. 5. The line at 3.7 ppm belongs to carbohydrate. Its intensity varies with the flow weighting. The fit of the spectral data at 3.7 ppm gives a velocity value of $213 \pm 20\,\mu m/s$. The so calculated carbohydrate flow velocity matches very well the water flow velocity in the phloem previously determined from flow imaging [9]. The second resonance at 2.7 ppm could not be assigned to a metabolite. Since the signal intensity does not change at different flow encoding strengths, it was therefore supposed to be stationary. The CSI data confirm this hypothesis. The map of the unknown metabolite shown in Fig. 6(d) indicates that this substance is not involved in the transport system of the plant since it can be found in the parenchyma only. In contrast, the carbohydrates are located in the phloem ring Fig. 6(c).

5. Discussion and conclusion

In this paper a strategy was proposed for the direct quantitative measurement of metabolite flow velocity in intact plants. For this purpose, flow sensitive preparation was combined with slice selective spectroscopy. The capability of this approach to quantify slow flow velocities of metabolites with low concentration was demonstrated in phantom studies. An example of an in vivo investigation was presented.

The high sensitivity of the spectroscopic approach enables it to directly quantify carbohydrate flow in an intact plant for the first time. Another advantage of this technique is that it allows flow to be measured in the phloem, even in plants were xylem and phloem cannot be resolved spatially.

Therefore, flow encoded spectroscopy not only offers the possibility of directly assessing carbohydrate flow but also of investigating phloem flow in many more plant species.

Acknowledgments

The authors want to thank K. Hartmann and A. Peuke (Botanischer Garten, Würzburg) for providing the plant material. Special thanks to A. Webb for reading the manuscript.

References

[1] M. Heidenreich, W. Köckenberger, R. Kimmich, N. Chandrakumar, R. Bowtell, Investigation of carbohydrate metabolism and transport in castor bean seedlings by cyclic *J* cross polarization imaging and spectroscopy, J. Magn. Reson. 132 (1998) 109–124.

[2] Y. Xia, P.T. Callaghan, "One-shot" velocity microscopy: NMR imaging of motion using a single phase-encoding step, Magn. Reson. Med. 23 (1) (1992) 138–153.

[3] P.T. Callaghan, W. Köckenberger, J.M. Pope, Use of difference propagators for imaging of capillary flow in the presence of stationary fluid, J. Magn. Reson. B 104 (1994) 183–188.

[4] E. Kuchenbrod, M. Landeck, F. Thürmer, A. Haase, U. Zimmermann, Measurement of water flow in the xylem vessels of intact maize plants using flow-sensitive NMR imaging, Bot. Acta 109 (3) (1996) 184–186.

[5] W. Köckenberger, J.M. Pope, Y. Xia, K.R. Jeffrey, E. Komor, P.T. Callahan, A non-invasive measurement of phloem and xylem water flow in castor bean seedlings by nuclear magnetic resonance microimaging, Planta 201 (1997) 53–63.

[6] M. Rokitta, U. Zimmermann, A. Haase, Fast NMR flow measurements in plants using FLASH imaging, J. Magn. Reson. 137 (1999) 29–32.

[7] T.W. Scheenen, D. van Dusschoten, P.A. de Jager, H. Van As, Microscopic displacement imaging with pulsed field gradient turbo spin-echo NMR, J. Magn. Reson. 142 (2000) 207–215.

[8] T.W. Scheenen, D. van Dusschoten, P.A. de Jager, H. Van As, Quantification of water transport in plants with NMR imaging, J. Exp. Bot. 51 (351) (2000) 1751–1759.

[9] M. Rokitta, A.D. Peuke, U. Zimmermann, A. Haase, Dynamic studies of phloem and xylem flow in fully differentiated plants by fast nuclear-magnetic-resonance imaging, Protoplasma 209 (1999) 126–131.

[10] A. Haase, M. Brandl, E. Kuchenbrod, A. Link, Magnetization-prepared NMR microscopy, J. Magn. Reson. A 105 (1993) 230–233.

[11] D. Bourgeois, M. Decorps, Quantitative imaging of slow coherent motion by stimulated echoes with suppression of stationary water signal, J. Magn. Reson. 94 (1991) 20–33.

[12] E.O. Stejskal, J.E. Tanner, Spin diffusion measurements: spin echoes in the presence of a time-dependent field gradient, J. Chem. Phys. 42 (1965) 288–292.

[13] H.S. Black, Modulation Theory, Van Nostrand, Princeton, 1953.

[14] P.T. Callaghan, Principles of Nuclear Magnetic Resonance Microscopy, Clarendon Press, Oxford, 1991.

[15] D. Bourgeois, M. Decorps, A new method for detection of ultra slow coherent motion using B0 gradients, in: Abstracts of 8th Annual Meeting, SMRM, Amsterdam, 1989, p. 1020.

[16] D.I. Hoult, R.E. Richards, Proc. Roy. Soc. (London) A344 (1975).

[17] G.H. Sørland, J.G. Seland, J. Krane, H.W. Anthonsen, Improved convection compensating pulsed field gradient spin-echo and stimulated-echo methods, J. Magn. Reson. 142 (2000) 323–325.

[18] Spektroskopie online, Internet: http://www.chem.uni-potsdam.d/tools/index_de.html, January 2002.

[19] W. Landschütz, M. Meininger, P.M. Jakob, F. Thürmer, U. Zimmermann, A. Haase, In-vivo functional NMR imaging on plants at 7 T, 13th ESMRMB 209 (1996) 125.

[20] A.D. Peuke, W. Hartung, W.D. Jeschke, The uptake and flow of C, N and ions between roots and shoots in *Ricinus communis* L. II. Grown low or high nitrate supply, J. Exp. Bot. 45 (1994) 733–740.